Optical properties of highly polarized InGaN light-emitting diodes modified by plasmonic metallic grating

Hong Chen, Houqiang Fu, Zhijian Lu, Xuanqi Huang, Yuji Zhao*

School of Electrical, Computer and Energy Engineering, Arizona State University, Tempe, AZ 85287, USA
*yuji.zhao@asu.edu

Abstract: We implement finite-difference time-domain (FDTD) method to simulate the optical properties of highly polarized InGaN light emitting diodes (LEDs) coupled with metallic grating structure. The Purcell factor (F_p), light extraction efficiency (LEE), internal quantum efficiency (IQE), external quantum efficiency (EQE), and modulation frequency are calculated for different polarized emissions. Our results show that light polarization has strong impact on F_p and LEE of LEDs due to their coupling effects with the surface plasmons (SPs) generated by metallic grating. F_p as high as 34 and modulation frequency up to 5.4 GHz are obtained for a simulated LED structure. Furthermore, LEE, IQE and EQE can also be enhanced by tuning the coupling between polarized emission and SPs. These results can serve as guidelines for the design and fabrication of high efficiency and high speed LEDs for the applications of solid-state lighting and visible-light communication.

OCIS codes: (230.3670) Light-emitting diodes; (250.5403) Plasmonics; (230.5440) Polarization-selective devices.

References and links

1. M. R. Krames, J. Bhat, D. Collins, N. F. Gardner, W. Götz, C. H. Lowery, M. Ludowise, P. S. Martin, G. Mueller, R. Mueller-Mach, and S. Rudaz, "High-Power III-Nitride Emitters for Solid-State Lighting," Phys. Status Solidi **192**(2), 237–245 (2002).
2. D. Feezell, S. S. James, P. D. Steven, and S. Nakamura, "Semipolar InGaN/GaN light-emitting diodes for high-efficiency solid-state lighting," J. Disp. Technol. **9**(4), 190–198 (2013).
3. F. Qian, S. Gradecak, Y. Li, C. Y. Wen, and C. M. Lieber, "Core/multishell nanowire heterostructures as multicolor, high-efficiency light-emitting diodes," Nano Lett. **5**(11), 2287–2291 (2005).
4. J. J. McKendry, R. P. Green, A. E. Kelly, Z. Gong, B. Guilhabert, D. Massoubre, E. Gu, and M. D. Dawson, "High-speed visible light communications using individual pixels in a micro light-emitting diode array," IEEE Photonics Technol. Lett. **22**(18), 1346–1348 (2010).
5. P. Waltereit, O. Brandt, A. Trampert, H. T. Grahn, J. Menniger, M. Ramsteiner, M. Reiche, and K. H. Ploog, "Nitride semiconductors free of electrostatic fields for efficient white light-emitting diodes," Nature **406**(6798), 865–868 (2000).
6. Y. Zhao, S. Tanaka, C. C. Pan, K. Fujito, D. Feezell, J. S. Speck, S. P. DenBaars, and S. Nakamura, "High-power blue-violet semipolar (2021) InGaN/GaN light-emitting diodes with low efficiency droop at 200 A/cm^2," Appl. Phys. Express **4**(8), 082104 (2011).
7. H. Fu, Z. Lu, X. Zhao, Y. H. Zhang, S. P. DenBaars, S. Nakamura, and Y. Zhao, "Study of low efficiency droop in semipolar (20-2-1) InGaN light-emitting diodes by time-resolved photoluminescence," J. Disp. Technol. (to be published).
8. Y. Zhao, S. H. Oh, F. Wu, Y. Kawaguchi, S. Tanaka, K. Fujito, J. S. Speck, S. P. DenBaars, and S. Nakamura, "Green semipolar $(20\bar{2}1)$ InGaN light-emitting diodes with small wavelength shift and narrow spectral linewidth," Appl. Phys. Express **6**(6), 062102 (2013).
9. Y. Zhao, Q. Yan, C. Y. Huang, S. C. Huang, P. S. Hsu, S. Tanaka, C. C. Pan, Y. Kawaguchi, K. Fujito, C. G. Van de Walle, and J. S. Speck, "Indium incorporation and emission properties of nonpolar and semipolar InGaN quantum wells," Appl. Phys. Lett. **100**(20), 201108 (2012).

#259477 Received 15 Feb 2016; revised 1 Apr 2016; accepted 9 Apr 2016; published 18 Apr 2016

10. Y. Zhao, R. M. Farrell, Y. R. Wu, and J. S. Speck, "Valence band states and polarized optical emission from nonpolar and semipolar III–nitride quantum well optoelectronic devices," Jpn. J. Appl. Phys. **53**(10), 100206 (2014).
11. H. Masui, H. Yamada, K. Iso, S. Nakamura, and S. P. DenBaars, "Optical polarization characteristics of InGaN/GaN light-emitting diodes fabricated on GaN substrates oriented between (1010) and (1011) planes," Appl. Phys. Lett. **92**(9), 091105 (2008).
12. M. Ueda, M. Funato, K. Kojima, Y. Kawakami, Y. Narukawa, and T. Mukai, "Polarization switching phenomena in semipolar In x Ga 1– x N/GaN quantum well active layers," Phys. Rev. B **78**(23), 233303 (2008).
13. M. Kubota, K. Okamoto, T. Tanaka, and H. Ohta, "Temperature dependence of polarized photoluminescence from nonpolar m-plane InGaN multiple quantum wells for blue laser diodes," Appl. Phys. Lett. **92**(1), 011920 (2008).
14. Y. Zhao, S. Tanaka, Q. Yan, C. Y. Huang, R. B. Chung, C. C. Pan, K. Fujito, D. Feezell, C. G. Van de Walle, J. S. Speck, S. P. DenBaars, and S. Nakamura, "High optical polarization ratio from semipolar (202 1) blue-green InGaN/GaN light-emitting diodes," Appl. Phys. Lett. **99**(5), 051109 (2011).
15. Y. Zhao, Q. Yan, D. Feezell, K. Fujito, C. G. Van de Walle, J. S. Speck, S. P. DenBaars, and S. Nakamura, "Optical polarization characteristics of semipolar $(30\bar{3}1)$ and $(30\bar{3}\bar{1})$ InGaN/GaN light-emitting diodes," Opt. Express **21**(101), A53–A59 (2013).
16. S. H. Park, D. Ahn, and S. L. Chuang, "Electronic and optical properties of a-and m-plane wurtzite InGaN–GaN quantum wells," IEEE J. Quantum Electron. **43**(12), 1175–1182 (2007).
17. W. G. Scheibenzuber, U. T. Schwarz, R. G. Veprek, B. Witzigmann, and A. Hangleiter, "Calculation of optical eigenmodes and gain in semipolar and nonpolar InGaN/GaN laser diodes," Phys. Rev. B **80**(11), 115320 (2009).
18. E. Matioli, S. Brinkley, K. M. Kelchner, Y. L. Hu, S. Nakamura, S. DenBaars, J. Speck, and C. Weisbuch, "High-brightness polarized light-emitting diodes," Light Sci. Appl. **1**(8), e22 (2012).
19. J. Vučković, M. Lončar, and A. Scherer, "Surface plasmon enhanced light-emitting diode," IEEE J. Quantum Electron. **36**(10), 1131–1144 (2000).
20. K. Okamoto, I. Niki, A. Shvartser, Y. Narukawa, T. Mukai, and A. Scherer, "Surface-plasmon-enhanced light emitters based on InGaN quantum wells," Nat. Mater. **3**(9), 601–605 (2004).
21. K. Okamoto, I. Niki, A. Scherer, Y. Narukawa, T. Mukai, and Y. Kawakami, "Surface plasmon enhanced spontaneous emission rate of InGaN/ GaN quantum wells probed by time-resolved photoluminescence spectroscopy," Appl. Phys. Lett. **87**(7), 071102 (2005).
22. I. Gontijo, M. Boroditsky, E. Yablonovitch, S. Keller, U. K. Mishra, and S. P. DenBaars, "Coupling of InGaN quantum-well photoluminescence to silver surface plasmons," Phys. Rev. B **60**(16), 11564 (1999).
23. X. Feng, F. Liu, and Y. Huang, "Calculated plasmonic enhancement of spontaneous emission from silicon nanocrystals with metallic gratings," Opt. Commun. **283**(13), 2758–2761 (2010).
24. D. Fattal, M. Fiorentino, M. Tan, D. Houng, S. Y. Wang, and R. G. Beausoleil, "Design of an efficient light-emitting diode with 10 GHz modulation bandwidth," Appl. Phys. Lett. **93**(24), 243501 (2008).
25. N. Gao, K. Huang, J. Li, S. Li, X. Yang, and J. Kang, "Surface-plasmon-enhanced deep-UV light emitting diodes based on AlGaN multi-quantum wells," Sci. Rep. **2**, 816 (2012).
26. E. M. Purcell, "Spontaneous emission probabilities at radio frequencies," Phys. Rev. **69**, 681 (1946).
27. Y. Xu, J. S. Vučković, R. K. Lee, O. J. Painter, A. Scherer, and A. Yariv, "Finite-difference time-domain calculation of spontaneous emission lifetime in a microcavity," J. Opt. Soc. Am. B **16**(3), 465–474 (1999).
28. E. Sakalauskas, Ö. Tuna, A. Kraus, H. Bremers, U. Rossow, C. Giesen, M. Heuken, A. Hangleiter, G. Gobsch, and R. Goldhahn, "Dielectric function and bowing parameters of InGaN alloys," Phys. Status Solidi, B Basic Res. **249**(3), 485–488 (2012).
29. D. Brunner, H. Angerer, E. Bustarret, F. Freudenberg, R. Höpler, R. Dimitrov, O. Ambacher, and M. Stutzmann, "Optical constants of epitaxial AlGaN films and their temperature dependence," J. Appl. Phys. **82**(10), 5090–5096 (1997).
30. E. K. Lau, A. Lakhani, R. S. Tucker, and M. C. Wu, "Enhanced modulation bandwidth of nanocavity light emitting devices," Opt. Express **17**(10), 7790–7799 (2009).
31. T. Suhr, N. Gregersen, K. Yvind, and J. Mørk, "Modulation response of nanoLEDs and nanolasers exploiting Purcell enhanced spontaneous emission," Opt. Express **18**(11), 11230–11241 (2010).
32. M. Nami and D. Feezell, "Optical properties of Ag-coated GaN/InGaN axial and core–shell nanowire light-emitting diodes," J. Opt. **17**(2), 025004 (2015).

1. Introduction

III-nitride InGaN light emitting diodes (LEDs) enable wide range of applications in solid-state lighting [1,2], full-color displays [3], and high-speed visible-light communication (VLC) [4]. Conventional InGaN quantum well (QW) LEDs grown on the polar *c*-plane orientation, however, suffer from quantum confined Stark effect (QCSE) due to the large internal polarization-related fields, which leads to a reduced radiative recombination rate and device efficiency. Furthermore, due to the tilted QW profile induced by QCSE, *c*-plane LEDs have larger carrier lifetime [5], which significantly limits their performance in achieving fast

#259477 Received 15 Feb 2016; revised 1 Apr 2016; accepted 9 Apr 2016; published 18 Apr 2016

modulation speed for high speed communication. To circumvent these negative effects, novel nonpolar and semipolar InGaN LEDs have been proposed and demonstrated with reduced QCSE, higher efficiency, and smaller carrier lifetime [6,7]. Other advantageous features including high efficiency, improved performance in green spectral region, and polarized emission, were also reported for nonpolar and semipolar devices [8–18].

Recently, surface plasmons (SPs) coupled emissions from LEDs have been proposed and demonstrated with improved efficiency and modulation speed [19–25]. Since the emission frequency of the InGaN/GaN QW is located near the resonance frequency of SPs at the metal/GaN interface, exploiting the plasmonic effect to enhance spontaneous emission is promising to further reduce the carrier lifetime for InGaN LEDs [20–23]. On the other hand, it has been reported that nonpolar and semipolar InGaN/GaN QWs have highly-polarized emission due to the separation of light hole (LH) band, heavy hole (HH) band and crystal-field split-off hole (CH) band [10–18]. Compared with conventional *c*-plane devices, optical properties such as F_P and carrier lifetime can be further enhanced by the polarized emissions from nonpolar and semipolar InGaN QW LEDs, because the coupling efficiency from the spontaneous emission to the surface plasmon modes is dependent on the transverse magnetic (TM) component of the light [24,25]. This *SPs-QW* coupling effects for polarized nonpolar and semipolar InGaN LEDs has never been explored and is the topic of this study.

In this work, we investigate the optical properties of highly polarized nonpolar and semipolar InGaN/GaN QW LEDs with metallic grating structure using finite difference time domain (FDTD) method. Key parameters such as Purcell factor (F_P), light extraction efficiency (LEE), internal quantum efficiency (IQE), external quantum efficiency (EQE), and modulation bandwidth will be studied systematically. The light source is simulated by classical dipoles and their orientations representing the polarized radiation from the QW. We find that all the optical properties are greatly impacted by the polarization emission coupled with SPs, and the device performance can be optimized by properly engineering the light polarization and metallic grating. The paper is organized as the following: in section 2, we describe the theoretical background and simulation methods; in section 3.1, F_P is calculated with various polarization and position of dipoles; in section 3.2, we study the LEE modified by the orientations and positions of the dipoles; in section 3.3 and 3.4, the device performance such as IQE, EQE, and modulation bandwidth are evaluated for the SPs enhanced InGaN LEDs.

2. Simulation method

2.1 Theoretical background

In 1946, Purcell proposed that the spontaneous emission can be enhanced by modifying its dielectric environment [26], where F_P is defined as the ratio between spontaneous emission rate modified by cavity and spontaneous emission rates in bulk. In FDTD method, F_P is calculated by the power ratio between the emitted power from a classical dipole surrounded by the cavity, and the power from the same dipole located in bulk material, which is proved to be equal the emission rate ratio [27]. In our simulation with grating structure, the Purcell factor F_P is given by:

$$F_P = \frac{3}{4\pi^2}\left(\frac{\lambda_c}{n}\right)^3\left(\frac{Q}{V}\right) = \frac{R_g}{R_0} = \frac{P_g}{P_0} \tag{1}$$

where λ_c is the wavelength in vacuum, n is the refractive index of bulk material, Q is the quality factor, V is the mode volume, R_g is the spontaneous emission rate with grating structure, and R_0 is the spontaneous emission rate in bulk material without grating. P_g and P_0 are the corresponding powers from the emitter inside the grating coated cavity and the emitter inside bulk material. FDTD method (from Lumerical FDTD Solutions) are employed in this

#259477 Received 15 Feb 2016; revised 1 Apr 2016; accepted 9 Apr 2016; published 18 Apr 2016

study to calculate the F_P as well as the power emitted from the top surface of the emitter, which will be described in section 3.1 and 3.2.

It is difficult to simulate the LEE of a realistic device because LEE is influenced not only by the metallic grating but also the substrate and the cavity geometry. Since the purpose of our research is to study the coupling between metallic grating and polarized emission, we define the LEE as the ratio between the emitted power measured above the metallic grating to the total power emitted by the dipole source inside the device, which will be normalized in the plots.

Combining the F_P and LEE, we further estimate the IQE and EQE in order to study the impact of metallic grating on device performance. Here we define the initial IQE and EQE of the QW emitter without metallic grating as IQE_0 and EQE_0, the IQE and EQE with the metallic grating structure as IQE_g and EQE_g, respectively. For the device with grating structure, the IQE_g is given by:

$$\mathrm{IQE}_g = \frac{F_P\ \mathrm{IQE}_0}{F_P\ \mathrm{IQE}_0 - \mathrm{IQE}_0 + 1} \tag{2}$$

The injection efficiency and the distribution of the carriers are also important to calculate the total EQE_g. The injection efficiency in this study is assumed to be unity. The carrier distribution is estimated using full lateral diffusion approach and no lateral carrier diffusion approach. In full lateral diffusion approach, we assume that the carriers are distributed uniformly across the lateral dimension, while for no lateral diffusion approach, the carriers are only uniformly distributed beneath the metal.

The photon emission inside QW is represented by dipoles with different orientations. For those nonpolar and semipolar InGaN QW LEDs, the emissions are not totally polarized along one direction, which is widely discussed in various literatures [10–15] by involving the polarization ratio $\rho = (I_\perp - I_\parallel)/(I_\perp + I_\parallel)$ with different definition of $I_\perp$ and $I_\parallel$. For InGaN with moderate indium composition, the light polarized vertical to the growth plane (TM polarized) is relatively weak compared with the in-plane polarized light (TE polarized). Thus light polarized vertical to the growth plane is assumed to be zero when we estimate the performance of InGaN LEDs grow on different planes. For simplicity, we only considered the polarization along the optimal direction and the polarization vertical to it. The polarization ratios as well as the main polarization directions of different polar, nonpolar and semipolar InGaN LEDs in our study are listed in Table 1.

Table 1. Polarization ratios and main polarization directions of different polar, nonpolar and semipolar InGaN LEDs

Plane	Polarization ratio (ρ)	Polarization direction	Reference
c-plane polar	0	No preference	[10]
$(10\bar{1}\bar{1})$ semipolar	0.55	$[\bar{1}2\bar{1}0]$	[11]
$(10\bar{2}\bar{2})$ semipolar	0.36	$(11\bar{0}\bar{0})$	[12]
$(20\bar{2}\bar{1})$ semipolar	0.6	$[\bar{1}2\bar{1}0]$	[13]
$(30\bar{3}\bar{1})$ semipolar	0.56	$[\bar{1}2\bar{1}0]$	[14]
m-plane nonpolar	0.9	$[\bar{1}2\bar{1}0]$	[15]

#259477 Received 15 Feb 2016; revised 1 Apr 2016; accepted 9 Apr 2016; published 18 Apr 2016

2.2 Set-up of the 3D simulation

The 3D simulation set-up is shown in Fig. 1(a). Perfectly matched layer (PML) boundaries are used to terminate the propagation of the electromagnetic field. The size of simulation region is 2.59 μm × 1 μm × 2 μm for *x*, *y* and *z* directions, respectively. We overlap the PML boundaries on *y*-*z* plane with the metal intentionally in order to define the dielectric function on the PML layer accurately. The *x*–*z* plane at the top is 200 nm above the grating structure. Each PML boundary has 8 layers. In order to measure the radiated power, the dipole is surrounded by a 12 nm × 12 nm × 12 nm small power monitor box. A power monitor is located 50 nm above the grating to measure the LEE at the surface. The convergence of all the set-ups mentioned above are rigorously tested in order to obtain accurate results with proper computing speed.

The coordinate system in our simulation is defined in Fig. 1(b). θ and ϕ are defined as the angles from TE_1 and TE_2 to TM oriented dipoles respectively, and φ is the in-plane rotation angle from TE_1 to TE_2. For typical QWs on nonpolar/semipolar planes with high polarization ratios (e.g., QWs on *m*-plane), θ and ϕ are equal to 0° approximately and the φ is dependent on how we design the grating structure. For QWs on *c*-plane or other planes with low polarization ratios, the device performance is approximated by considering the emission from two or more dipoles with different φ and different weight factors. For QWs with high indium composition or extra strains, the θ and ϕ are no longer 0° and could be engineered [25].

The simulated structure is an InGaN/GaN QW coupled with a silver grating with period of 400 nm and duty circle of 50%. The parameters are not optimized but can give moderate performance based on our preliminary study. The p-type layer and the width of well are 12 nm and 3 nm, respectively. The indium composition is chosen to emit light at wavelength of 470 nm. The dielectric function of InGaN and GaN can be found in Ref [28]. and [29], respectively. For the dielectric function of silver, we choose the built-in Palik model in the Lumerical FDTD solutions. The spontaneous emission is represented by radiation from a classical dipole source located at the center of the QW, which has a central wavelength of 470 nm with finite linewidth. The highly polarized radiation from QW is simulated by dipoles with different orientations.

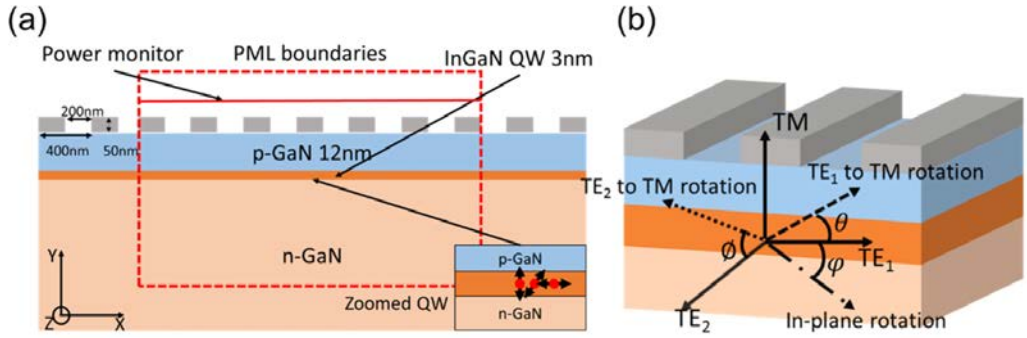

Fig. 1. (a) The schematic view of GaN/InGaN QW with silver grating. The period of the grating is 400 nm with 50% duty circle. The dash box indicates the FDTD simulation region. All of the materials are homogenous along the z direction. (b) The schematic view for different polarizations and rotations studied in this work. θ is polarization angle between TE_1 and TM; ϕ is the polarization angle between TE_2 and TM; φ is the polarization between TE_1 and TE_2.

#259477 Received 15 Feb 2016; revised 1 Apr 2016; accepted 9 Apr 2016; published 18 Apr 2016

3. Results and discussion

3.1 Purcell factor

In this section, we study the light emission from dipoles with different orientations at different locations. The orientation of TE_1, TE_2, and TM dipoles are defined below, where location A and C refer to the dipole located at the center of the gap and the center of sliver stripe, while B refers to the dipole located beneath the edge of the silver stripe. Different rotations are defined in Fig. 1(b).

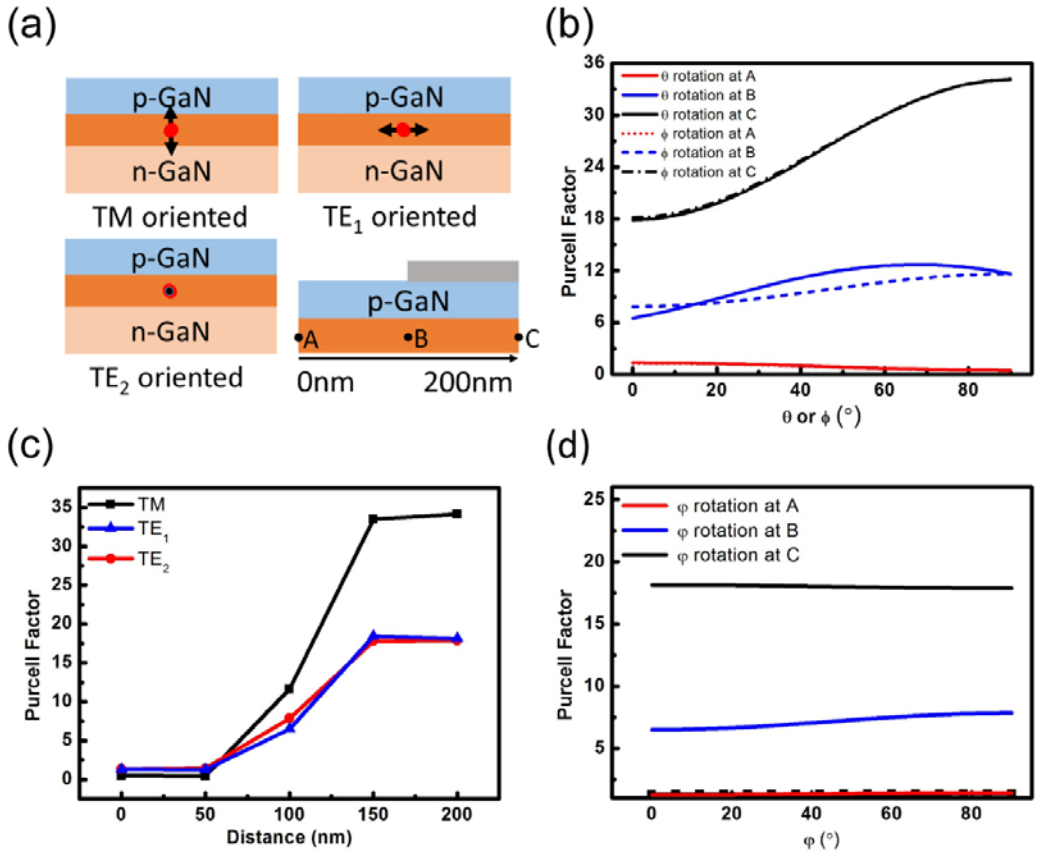

Fig. 2. (a) The schematic views for the TE_1, TE_2 oriented dipoles. Position A is at the center of the gap between metal strips; position B is at the edge of the metal strip, and position C is at the center of metal strip. (b) F_P of the dipoles located at A, B and C with different orientation. 0, 90 degrees indicate the TE_1/TE_2 oriented dipole and TM oriented dipole, respectively. (c) Distribution of F_P along *x* axis. (d) F_P of the dipoles rotate in-plane located at A, B and C.

Figure 2(b) shows the F_P as a function of dipole orientation. For dipoles located at position A, a large increasing of F_P is observed if the θ and ϕ are increased. Such an increase of F_P is also observed in structure with silver thin film (result not shown). With increased θ and ϕ, the TM radiation component towards the metal/semiconductor interface becomes larger. Since the SPs can be coupled with TM radiation component more efficiently, higher F_P could be achieved when θ and ϕ are increased. Previous theoretical studies only considered the light polarization directions of InGaN LEDs to be random and averaged all the directions when calculating the optical properties [22,23]. This could lead to an overestimation of the F_P since only one dominant polarization exist in most highly polarized InGaN LEDs.

#259477 Received 15 Feb 2016; revised 1 Apr 2016; accepted 9 Apr 2016; published 18 Apr 2016

Furthermore, when the dipole is located at A and B, the distance between dipoles and the metal stripe increases, thus the coupling efficiency between the spontaneous emission and the SP modes decrease. For position A, since dipoles are more than 100 nm away from the metal, the plasmonic effect is relatively weak. And the reflected spherical wave from the top surface 12 nm above will have strong "interference" with the dipole source in the simulation, leading to different radiated power through constructive or destructive "interference". Such numerical phenomenon does not happen in reality but is corresponding to the manipulated photon lifetime, or equivalently, the manipulated quality factor (Q) for the radiative mode beneath the metallic grating. For TE_1 and TE_2 oriented dipoles at position A, the F_p is higher than that of the TM oriented dipoles since it avoids the destructive "interference" which result in lower quality factor. Moreover, F_P smaller than 1 is observed for TM oriented dipoles at position A (F_P = 0.49), which is owing to the destructive "interference" between reflected wave from the top layer and dipole source in the FDTD simulation. For TE_1 dipoles at position B, maximum F_P is achieved around $\theta = 60°$ instead of $90°$, which is resulted from the larger TM radiation component towards the metal/semiconductor interface when $\theta = 60°$. In Fig. 2(c), we map the F_P with different locations on x direction. As the dipole is moving towards the center of silver strip, the F_P increases due to the increased mode coupling efficiency.

We also studied the effect of in-plane rotation on the F_P. Figure 2(d) shows that F_P is almost constant when the dipole is rotating in-plane at A and C due to the invariant TM component. For dipoles located at B, the F_P is rotation-dependent since the silver stripe is no longer right above the dipole geometrically.

In a short summary, F_P is determined by two different mechanisms, for those dipoles located at C, the plasmonic effect is strong. F_P is determined by the mode coupling efficiency and is increasing with θ and ϕ. For dipoles at A, the plasmonic effect is relatively weak, and the TE oriented dipoles give higher quality factor to the radiative mode since it avoid destructive "interference". Thus F_P decreases with θ and ϕ. The simulation on F_P also shows that the F_P will decrease when the dipole is moved away from the metal stripe due to reduced coupling efficiency to plasmonic modes. In reality, even though the TM emission component of InGaN LEDs is relatively low when indium composition is moderate, it's still possible to add extra strains in the QWs to get more TM components [24] to achieve higher modulation speed.

3.2 LEE

In this section, we simulate the LEE of devices with different polarized emissions. The simulation configurations and the definitions of the locations and rotations are the same as we used in the previous discussion. In the simulation, LEE is defined as the ratio of radiated power through metallic grating to the total power emitted from the dipole. In order to clarify how grating structure manipulates the polarized emissions, we normalized the LEE to the highest value which is achieved at position A by TE dipoles.

Figure 3(a) shows LEE as a function of dipole orientation at position A, B and C. At position C, LEE decreases with increasing dipole orientation angle ϕ or θ. With larger ϕ or θ, TM polarization component is dominant which leads to a stronger *SPs-QW* coupling. However, radiation coupled with plasmonic modes do not contribute to the power extraction due to the localized electromagnetic field, which results in the reduction of LEE. For dipoles locate at position A, since the dipole is far away from the metal stripe, the plasmonic effect is relatively weaker compared to the case at position C. Therefore the extraction mechanism is dictated by the reflection of light at the surface. In addition, we also compare the LEE results to the cases without grating structures. The result shows that at position A, the LEE without grating structure is 1.01 for the TE dipole and is 0.946 for the TM dipole under the same normalization condition. This indicate that the grating structure performs as a scattering object which balances the metal loss by enhancing the LEE. Figure 3(b) shows that there's a large

#259477 Received 15 Feb 2016; revised 1 Apr 2016; accepted 9 Apr 2016; published 18 Apr 2016

difference between the LEE of TE_1 and TE_2 oriented dipole (0.115 for TE_1 and 0.058 for TE_2). This is due to the fact that for TE_1 the radiation from the dipole is propagating along the direction with grating periodicity, while for TE_2 the direction is along the metal strip thus has lower chance to be scattered out. Figure 3(c) further verified such deduction by showing the mapped LEE with the distance from A to C. At the edge of the grating (position B) the LEE of TM oriented dipole is higher than TE_2 oriented dipole, meaning the SPs could be scattered into free propagating photons efficiently. By efficiently coupling the spontaneous emission to the SPs then efficiently scattering the SPs out as suggested in Ref [25], the LEE could be enhanced by plasmonic effect.

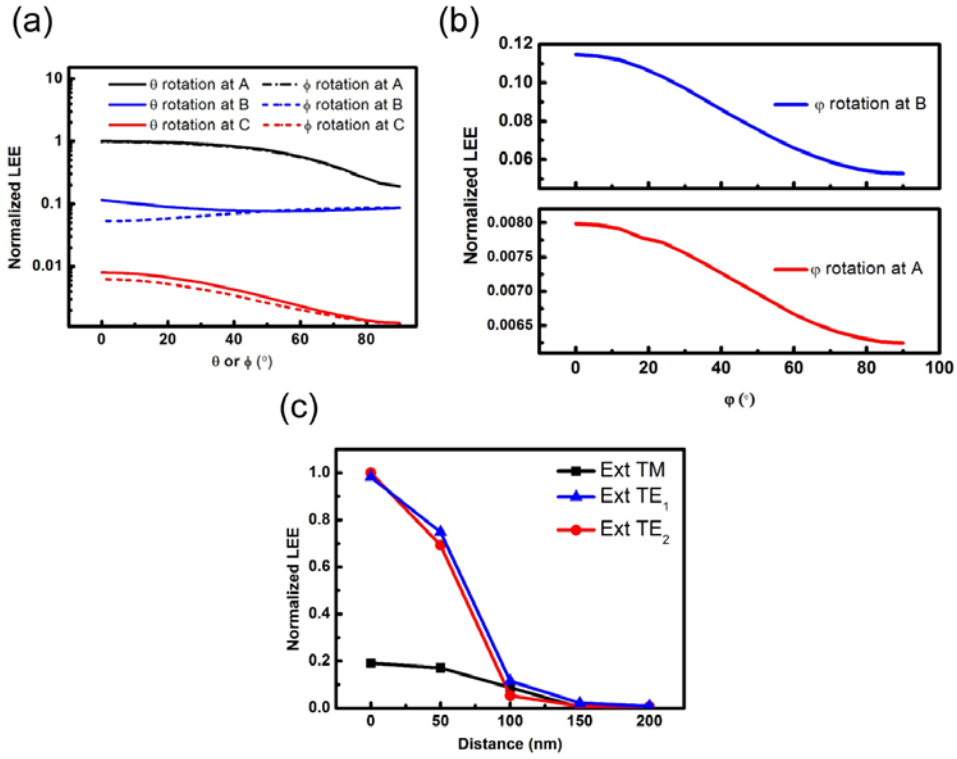

Fig. 3. (a) The normalized LEE of dipoles located at A, B, and C with different orientations. Dipoles are rotated by changing θ and ϕ. (b) The normalized LEE of the dipoles located at A, B, and C with different orientations. Dipoles are rotated by changing φ. (c) Mapped normalized LEE along *x* axis.

In a short summary, dipoles perpendicular to the grating stripe (TE_1) has higher LEE than dipoles parallel to the grating stripe (TE_2). These results can help us to improve the LEE of InGaN/GaN QWs based devices where the optical transitions are TE_1 and/or TE_2 oriented. Since the F_P of TE_1 and TE_2 oriented dipoles are almost the same, by carefully designing the orientation of the polarized radiation from QW and the metallic grating, we will be able to achieve a high LEE while keeping a moderate F_P at the same time.

3.3 IQE and EQE

In this section, we study in detail how the IQE_g and EQE_g of devices can be modified by the interaction between metallic grating and polarized emission. The definitions of locations and dipole rotations are the same as we used in the previous section. In reality, the lateral carrier diffusion and the non-uniform recombination rate due to the Purcell effect will influence the

#259477 Received 15 Feb 2016; revised 1 Apr 2016; accepted 9 Apr 2016; published 18 Apr 2016

carrier distribution. For simplicity, the full lateral diffusion approach and no lateral diffusion approach is employed for this work as we discussed in the previous section. Figure 4(a) shows the IQE_g at position A, B and C as a function of IQE_0. IQE_g at position C is higher than that at position B due to stronger *SPs-QW* coupling effects. At the same position, the IQE enhancement for TM polarization is larger than other polarizations, which can be attributed to the larger F_p of TM polarization as shown in Fig. 2(c). Although IQE_g is larger than IQE_0, the enhancement of IQE (IQE_g/IQE_0) decreases with increasing IQE_0, indicating that Purcell effect will enhance LEDs with relatively low IQE_0 more effectively. Figure 4(b) gives the estimated normalized EQE_g at position A, B and C. All of the values are normalized to the EQE_g of TE_2 oriented dipoles at position A with $IQE_0 = 0.9$. When IQE_0 is larger than 0.2 which is almost always the case for InGaN LEDs, TE polarized dipoles has the highest EQE_g at all of the locations due to its highest LEE and moderate F_P. To give a more accurate estimation, we integrated EQE_g over all space and the results are shown in Fig. 4(c). For TE_1 polarized emission, the integrated EQE_g is 2.5 times higher than that of the TE_2 polarization without lateral carrier diffusion, even though the F_P are almost the same for these two polarization. Such observation is potentially important for the design of high speed LED since a high F_P and moderate LEE is desirable in such device. When lateral carrier diffusion is considered, the EQE_g of TE_1 oriented dipole is till 1.14 times larger than that of TE_2 dipoles, which is attributed to the large difference in LEE at position B. The performance of the real device is highly dependent on the carrier distributions within the active layer, which is influenced by the lateral diffusion and the non-uniform recombination rate across the active layer. Moreover, since the light radiated from the nonpolar/semipolar InGaN/GaN QW is strongly polarized, the orientation between the dipoles and the metallic gratings might have significant impacts on the EQE_g performance of these device.

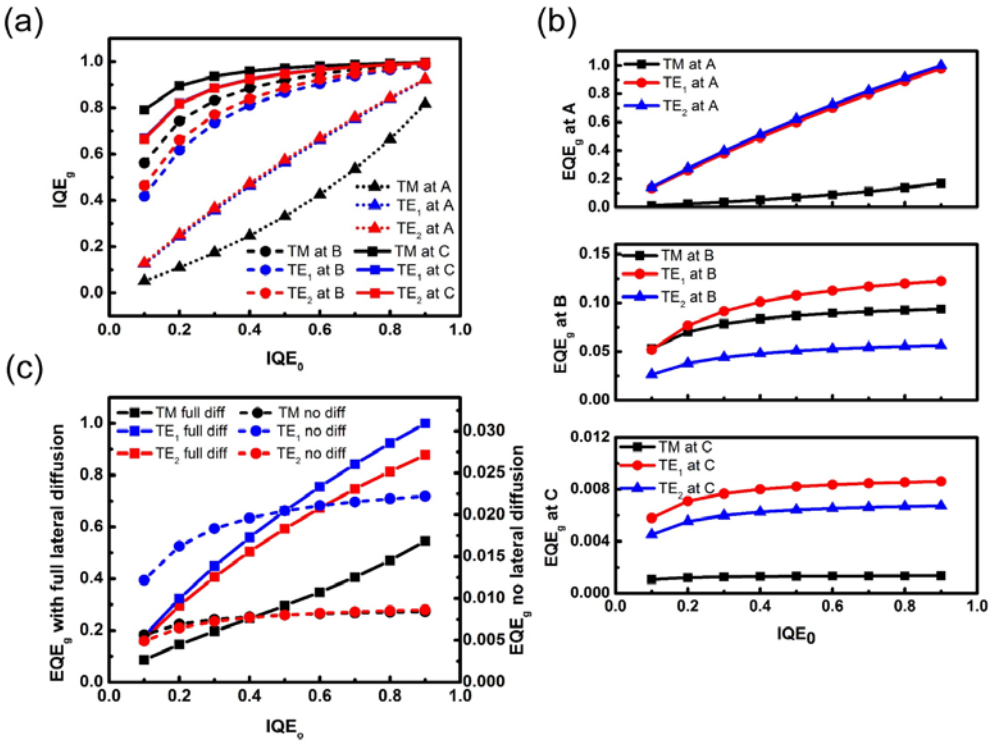

Fig. 4. (a) IQE_g with metallic grating as a function of IQE_0 at A, B and C. (b) EQE_g with grating structure as a function of IQE_0 at A, B and C. (c) The integrated EQE_g over all space versus IQE_0 for cases of full lateral diffusion and non-lateral diffusion.

#259477 Received 15 Feb 2016; revised 1 Apr 2016; accepted 9 Apr 2016; published 18 Apr 2016

3.4 Device performance

The modulation speed of LEDs and LDs on nanoscale are theoretically analyzed in Ref [30,31]. The calculation in [31] shows that the modulation speed is almost *Q* independent due to the balancing between the large F_P and the narrow Lorenzian of cavity mode. For QW LEDs, the highest achievable modulation speed is limited to tens of GHz due to the strong cavity effect. However, the *Q* factor of our simulated structure is relatively small due to the weak cavity confinement, which eliminates the restraints on the modulation frequency. In our device, the Purcell effect is a result of shrinking the mode volume by the plasmonic effect, which might potentially provide another path to increasing modulation speed.

For the carriers inside the QW, the lifetime modified by Purcell effect can be estimated by [32]:

$$\frac{1}{\tau_{\text{eff}}} = \frac{F_P}{\tau_{\text{r}}} + \frac{1}{\tau_{\text{nr}}} \tag{3}$$

where τ_{r} is radiative recombination lifetime, τ_{nr} is the non-radiative recombination lifetime, and τ_{eff} is the effective recombination lifetime. Considering the cavity confinement, the 3dB frequency can be written as [31,32]:

$$f_{\text{3dB}} \approx \frac{1}{2\pi} \frac{1}{\sqrt{\tau_{\text{p}}^2 + \tau_{\text{eff}}^2}} \tag{4}$$

where $\tau_{\text{p}} = Q / \omega_0$ is the lifetime of photons inside the cavity. For device with strong cavity effect, the *Q* factor is extremely high and the photon lifetime will restrict the modulation speed of device. For device with weak cavity effect (our case), the *Q* factor is relatively small and the τ_{p} is negligible. Using proposed approach, we estimated the EQE_{g} and the modulation bandwidth with different dipole orientations for nonpolar *m*-plane InGaN LEDs and the results are presented in Table 2. The radiative recombination lifetime of nonpolar *m*-plane LED is chosen to be τ_{r} = 0.45 ns as measured in Ref [5]. using the time resolved photoluminescence (TRPL) method, the non-radiative recombination lifetime is chosen to be τ_{nr} = 0.5 ns as analyzed in Ref [32]. For *m*-plane InGaN/GaN device, modulation speed from 3.5 GHz to 5.4 GHz is achievable if the grating and the growth plane is carefully oriented.

Table 2. Device performance of nonpolar *m*-plane InGaN LEDs with different dipole orientations

Dipole orientation	Purcell factor (full lateral diffusion)	Purcell factor (no lateral diffusion)	Normalized EQE_{g} with full/no lateral diffusion	Bandwidth with full/no lateral diffusion (GHz)
TM	16.4	26.4	0.54 / 0.0084	6.0 / 9.7
TE_1	9.1	14.4	1.00 / 0.0224	3.5 / 5.4
TE_2	9.2	14.5	0.88 / 0.00865	3.6 / 5.5

As shown in Table 1 in the previous section, the polarization ratios are not unity in nonpolar and semipolar QWs. Therefore the emission cannot be totally polarized at the optimal direction. However, it is quit intuitive that with a large polarization ratio, more emissions could be efficiently polarized at the TE_1 direction where the highest total EQE is observed, leading to better overall device performance. Therefore the *m*-plane LED performs

#259477 Received 15 Feb 2016; revised 1 Apr 2016; accepted 9 Apr 2016; published 18 Apr 2016

better compared with devices on other orientations since it has the largest polarization ratio. The estimated EQE_g for polar, nonpolar and semipolar InGaN LEDs are summarized in Table 3, where the EQE_g are normalized to the *m*-plane device values for both the cases of full lateral diffusion and no lateral diffusion.

Table 3. Estimated EQE_g for polar, nonpolar and semipolar InGaN LEDs

Plane	Estimated EQE_g with full/no lateral diffusion
c-plane polar	0.95 / 0.72
$(10\bar{1}\bar{1})$ semipolar	0.98 / 0.89
$(10\bar{2}\bar{2})$ semipolar	0.97 / 0.82
$(20\bar{2}\bar{1})$ semipolar	0.98 / 0.90
$(30\bar{3}\bar{1})$ semipolar	0.98 / 0.89
m-plane nonpolar	1 / 1

For the EQE_g with full lateral carrier diffusion, QWs on different planes show similar performance. For the EQE_g without lateral carrier diffusion, the nonpolar *m*-plane device showed much higher performance compared to polar *c*-plane device. Since the effective F_p is 14.5 beneath the metal, the radiative recombination rate is much higher beneath the metal. Therefore in real devices, we can expect that more carriers will be recombined beneath the metal, leading to a higher EQE_g at TE_1 direction compared to TE_2. Thus the devices based on *m*-plane could provide more output power compared to other devices due to the high polarization ratio and the large radiative recombination rate beneath metal.

4. Conclusion

We simulate the Purcell factor F_P, LEE, IQE, EQE and modulation frequency of InGaN/GaN QWs LEDs coupled with silver grating, which not only supports the plasmonic mode but also enables electrical injection. Results indicate that *SPs-QW* coupling strongly impacts highly-polarized emission from the InGaN QW as well as the LED device performance. First of all, TM polarization has largest F_P and smaller LEE compared with TE polarization. This is because F_P is related to plasmonic mode with non-radiative property, while LEE is mainly determined by the coupling efficiency to radiative mode. Second, the distance between SPs and dipole also impacts F_P and LEE. By moving the dipole away from grating, the coupling becomes weak (smaller F_P) while LEE increases for TE polarized dipoles. This is due to the competition between plasmonic mode and radiative mode. At the edge of the grating, the LEE of TE_1 dipole is 2 times higher than that of the TE_2 dipole due to their different radiation directions. Third, the in-plane polarization (TE_1 and TE_2) shows minimum change in F_P while LEE highly depending on the rotation of dipole. TE_1 polarization shows higher LEE than TE_2 polarization, which means TE_1 polarization is more efficient emitter with higher EQE. Such observation might potentially guide the design of highly polarized InGaN QWs for high speed LEDs, which is dominated by TE polarization. In this calculation, the achievable modulation speed is up to 5.4 GHz. The highest EQE is achieved using nonpolar *m*-plane InGaN QW due to its largest polarization ratio. In addition, carrier distribution also plays an important role in the device performance. Further investigations are required to simulate more realistic device structures (e.g. multi-QW structures), and study the trade-off between the high modulation speed and the output power of the LEDs.

#259477 Received 15 Feb 2016; revised 1 Apr 2016; accepted 9 Apr 2016; published 18 Apr 2016

Acknowledgment

This work is supported by Bisgrove Scholar Program from Science Foundation Arizona.

#259477 Received 15 Feb 2016; revised 1 Apr 2016; accepted 9 Apr 2016; published 18 Apr 2016